ON THE DEVELOPMENT OF A REAL-TIME SIMULATOR ENGINE FOR A HYDRAULIC FORESTRY MACHINE

Evangelos Papadopoulos[1] and Yves Gonthier[2]

[1] Dept. of Mechanical Engineering, National Technical University of Athens, 15780 Athens, Greece
[2] Canadian Space Agency, St. Hubert, PQ, Canada J3Y 8Y9
egpapado@central.ntua.gr

Abstract

This work focuses on the development of a real-time training simulator engine for a forestry machine. The rigid body dynamics of the machine's manipulator is integrated with electrohydraulic actuator dynamics and joint controllers. System numerical stiffness introduced by the closing valves, high order hydraulic dynamics, and simulator implementation using an interpreted language were identified as the prime reasons for slowing down the integration. Successive models of lower complexity and switching between models for the open and closed phases of the valves are proposed aiming to achieve a satisfactory simulator engine that can run in real-time. Simulation results demonstrate very good prediction of an actual machine behaviour with execution speeds improved by a factor of 35.

Keywords: machine training simulator, hydraulic dynamics, numerical stiffness, real-time, control system

1 Introduction

Forestry is Canada's most important industry in terms of people employed and contribution to the economy (Courteau, 1994). Increased competition from overseas and strict environmental laws require that forestry resources are harvested more efficiently and more carefully than previously done. This competition requires improved forestry equipment, for example lightweight and efficient machines with more user-friendly controls and self-diagnostics, and machine operators who can be trained more quickly and at a lower cost (Freedman et al, 1995). Such training can be greatly facilitated by the use of machine graphical simulators.

Presently, forestry machine training relies on the use of actual and expensive machines (Freedman et al, 1997). This dependence decreases training efficiency, and increases the cost due to trainee-induced machine breakdowns. The availability of an inexpensive simulator can increase the throughput, and prepare the trainees sufficiently well before working with an actual machine. Although aviation simulators have existed for long time, it is only in recent years that simulators in the areas of medicine (Ruspini, 2000), space (Piedboeuf, 1999), underwater robotics (Choi, 2001), nuclear industry (Mort et al, 1997), or heavy machines (Lawrence et al, 1993; Yoneda et al, 1997) have appeared.

The need to reduce the cost of simulators results in dynamic plant simplifications that usually deteriorate the realism and effectiveness of a training simulator. For example, simulators for forestry machines are based usually on manipulator kinematics. To improve the simulation quality to some extent the realism, the rigid body dynamics, the rigid body dynamics that describes the pendulum motion of a harvester head is taken into account (Freedman, 1999). The coupled manipulator rigid-body dynamics and electrohydraulic actuator dynamics are still ignored.

The work described in this paper is concerned with the development of a real-time simulator for a harvester, i.e., a forestry machine that fells and processes trees, see Fig.1. In order to perform this task, one first needs to model the machine and its manipulator both kinetically and dynamically, and to obtain key parameters (Papadopoulos and Sarkar, 1997; Papadopoulos et al, 1997). However, the derived models tend to be very complicated and hard to implement on a real-time basis. Therefore, additional simplifications and techniques are required to achieve this goal.

In this study, methods that enable simulation of an electro-hydraulically actuated mechanical manipulator in real time are proposed. The manipulator rigid body equations of motion are integrated into the Linear Graph-based state equations that describe the dynamics of the electrohydraulic actuators, and a complete model of the actuation system is developed that can produce both forward and backward joint motions. The same controller that is used on the actual experimental forestry machine in Fig. 1, is also integrated with the system dynamics to generate valve control voltages. Numerical stiffness and state discontinuity problems related to valve closure/opening are described and solutions are proposed. To accelerate simulation execution, a reduced model of the electrohydraulic actuators is proposed. The fluid line dynamics is eliminated and the hydraulic actuation system is modelled as a purely resistive network. Continuity of state variables is ensured. The response of full and reduced models are compared and found to be in excellent agreement. More importantly, the methods presented here indicate that a real-time implementation of a simulator is possible.

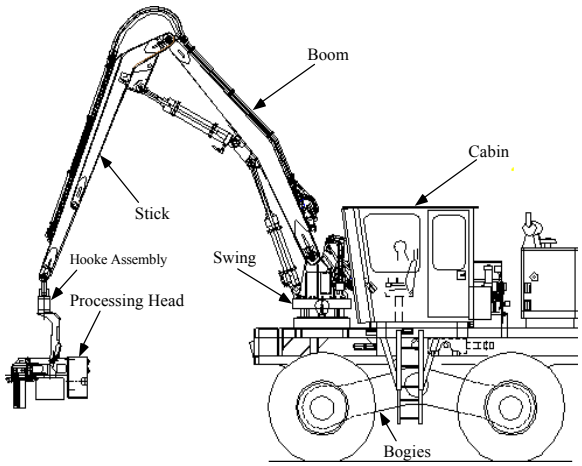

Fig. 1: *The experimental forestry machine*

2 Dynamics & Control Simulator Engine

A satisfactory dynamic simulator of a hydraulically actuated forestry machine, requires an accurate model of its rigid body dynamics, hydraulic actuation subsystem, and its control algorithm. Preliminary models of the manipulator and actuation subsystems were introduced in previous works (Papadopoulos and Sarkar, 1997; Papadopoulos et al, 1997). The parameters for those models were determined experimentally (Papadopoulos et al, 1997). The subsystem models were interfaced to result in dynamic models describing the behaviour of the full-system to open-loop commands. However, from the point of view of simulator design, these models were subject to some limitations. The modelling process that was employed is briefly addressed next.

a. Hydraulic Actuation System Modelling

The manipulator hydraulic actuation subsystem activates three degrees-of-freedom (dof) which correspond to the swing, stick, and boom motions, see Fig.1. Each subsystem model takes into account the pump (a variable displacement pressure), the transmission lines (hoses), a proportional valve, and a cylinder or a hydraulic motor, depending on the actuation subsystem. Small losses due to filters or other hydraulic components are lumped with valve losses.

The models were developed using Linear Graph methodology (Rowell and Wormley, 1997). This methodology allows the systematic generation of system state-space equations of uni-dimensional lumped systems that may span various energy domains such as mechanical, electrical, fluid, etc. The methodology's name is derived from the fact that all basic elements are represented by directed linear segments. Despite its name, the methodology works well with nonlinear elements.

The topology of a system linear graph follows the topology of the real system that it describes. This is in contrast to Bond Graphs which represent the flow of energy in a multi-domain system (Rosenberg and Karnopp, 1983). The form of the linear graph of an electric circuit is basically the circuit itself, where each resistor, capacitor and inductor is replaced by a directed linear segment, whose direction shows the assumed positive current direction, while its terminals are connected to graph nodes that correspond to circuit nodes. In contrast to this, the Bond Graph of a circuit does not resemble at all the circuit itself.

Linear Graphs employ power variables, i.e. variables that their product gives power. These are divided in Across and Through variables. Across variables include those variables that are measured across two terminals or points and include voltages, velocities, pressures, temperatures, etc. Through variables include those variables that are measured by some medium interruption and include currents, forces, flows, heat, etc. A Linear Graph transformer is an element that converts an across variable in one domain to an across in another domain, while a gyrator converts it to a through variable. For example, a hydraulic cylinder converts pressure (across) to a force (through) and therefore is a gyrator. Due to these definitions, devices represented by a gyrator in Linear Graphs may be represented by a transformer in Bond Graphs.

Once a system linear graph is constructed, a minimum set of independent state equations is derived systematically. To this end, one uses three sets of equations, namely the elemental equations describing the element function (i.e. Ohm's law), and the com-

patibility and continuity equations (i.e. Kirchoff's laws) (Rowell and Wormley, 1997).

In hydraulic systems, graph nodes correspond to distinct pressures in a hydraulic circuit. Elemental equations describe the relationship between pressure and flow for the elementary hydraulic elements such as the inertial, capacitor, and resistive element denoted by I, C, and R, respectively. Compatibility equations result in pressure drop equations along a closed hydraulic circuit, while continuity equations result in flow continuity at system nodes or system closed surfaces.

To illustrate the methodology employed, the model for the swing actuation subsystem is described in some detail. This includes a constant pressure power supply, modelled as a source of pressure, transmission lines, modelled as an inertance, a resistance and a capacitance connected in a T configuration, a valve, modelled as a nonlinear resistance modulated by an input voltage or current to the valve torque motor, and a motor, modelled by a gyrator. The motor also includes internal and external leakages. More details about the choice of these elements and their interconnections can be found in (Papadopoulos et al, 1997).

Figure 2 shows the corresponding linear graph. The nodes a, b, c, etc. correspond to hydraulic circuit points with distinct pressure. Node d is the reference node, assumed to be at zero bar. Node c is at pump pressure. The line is modelled by a capacitance C_1, an inertance I_1 and a resistance R_1. Index 1 corresponds to the forward line, while index 2 corresponds to the return line. Node a corresponds to the pressure of some intermediary hose point. The proportional valve is represented by two variable nonlinear resistances, indicated by C_{R1} and C_{R2}. Nodes e and f correspond to the inlet and outlet ports of the hydraulic motor. The resistances R_{in}, R_{e1}, R_{e2} correspond respectively to the internal leakage and to the external leakages from the inlet and outlet ports to tank. A gyrator (hydraulic motor displacement D_m), describes the ideal hydraulic motor, and connects the hydraulic domain to the mechanical domain. The angular velocity at node j is the angular velocity of the motor's shaft. This is transformed via a gearbox with gear ratio N to the swing angular velocity denoted by $\dot{q}_{sw}$. The four linear segments between nodes l and k correspond to (a) the torque provided by the motor (segment 4), (b) the viscous torque (segment B_m), (c) the inertial torque accelerating inertias (segment J_{eq}), and (d) to an external torque that models the inertial and other coupling torque effects of the manipulator (segment T_S).

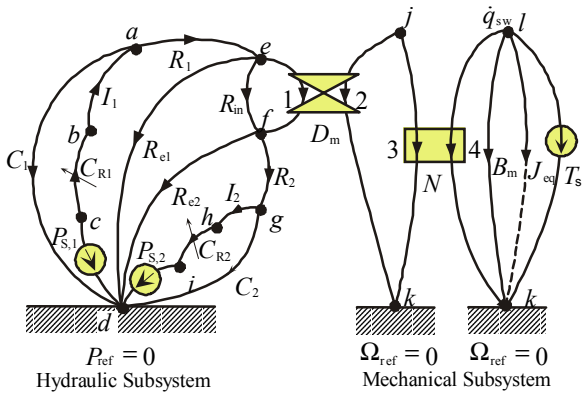

Fig. 2: *The swing actuator full model*

The modelling of the boom and stick actuation subsystems follows the same principles. Fig. 3 depicts the Linear Graph for a double-acting single-ended cylinder driving a rigid link, see also Fig. 4. Since the piston areas are not equal, two gyrators with areas A_1 and A_2 are used. Each gyrator describes the conversion of chamber hydraulic pressure to mechanical force. The lines (hoses) to and from the cylinder are modelled as in the swing case. The mechanical subsystem includes the viscous coefficient B_p, the equivalent cylinder mass M_{eq}, and all other coupling force terms, denoted by F_s. The modelling of these systems is described in more detail in (Papadopoulos et al, 1997).

Following this methodology, twelve nonlinear differential equations have resulted for the hydraulic actuation subsystem (Papadopoulos et al, 1997). However, these equations did not allow for both forward and backward motions of the manipulator, and therefore could not be used as such in a simulator.

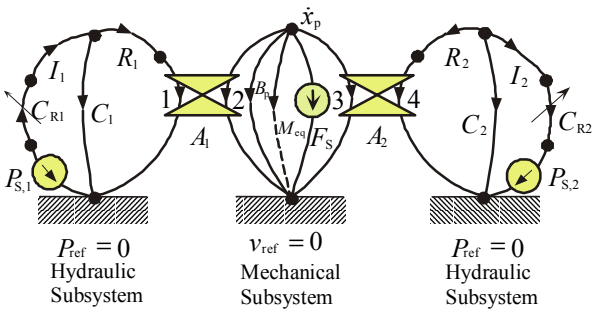

Fig. 3: *The cylinder actuator full model*

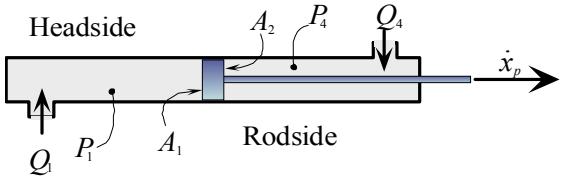

Fig. 4: *A hydraulic cylinder actuator*

b. Modelling of general actuator motions

Note that in hydraulic systems, motion is controlled with control flow valves, such as proportional spool-type valves. Each valve can be considered of as two orifices through which fluid flows. The pump draws oil from the tank and directs it through a valve orifice and a line to a cylinder or a hydraulic motor and back from the actuator through the line and the other valve orifice into the oil tank. An input voltage controls the spool position, which modulates valve orifice areas, and hence orifice resistance to the flow.

In simulation, to enable both forward and backward motions of a link, i.e., to have the sign of the swing angular velocities Ω or piston linear velocities $\dot{x}_p$ changed, the valve must be able to reverse the oil flow direction, as required by the swing motor and piston gyrator equations

Swing gearbox:

$$\begin{aligned} \Omega_3 &= \Omega_2 = N\,\Omega_4 = N\,\dot{q}_{\mathrm{sw}} \\ \tau_{\mathrm{sw}} &= \tau_4 = -N\,\tau_3 \end{aligned} \tag{1}$$

Swing motor:

$$\begin{aligned} Q_1 &= D_{\mathrm{m}}\Omega_2 \\ \tau_2 &= \tau_3 = -D_{\mathrm{m}}P_1 \end{aligned}$$

Headside piston:

$$\begin{aligned} Q_1 &= A_1\,v_2 = A_1\,\dot{x}_{\mathrm{p}}, \\ F_2 &= -A_1\,P_1 \end{aligned} \tag{2}$$

Rodside piston:

$$\begin{aligned} Q_4 &= -A_2\,v_3 = A_2\,\dot{x}_{\mathrm{p}}, \\ F_3 &= A_2\,P_4 \end{aligned}$$

where N represents gearbox ratio, D_{m} hydraulic motor displacement, Q flow rate, P pressure, F force, the subscript p indicates piston variables, and should be replaced by *bm* or *sk* for boom or stick respectively, the subscript *sw* indicates swing variables, x_{p} represents piston displacement, and the indices 1, 2, 3, and 4 correspond to variables associated with gyrator or transformer segments, see also Fig. 2 and 3. The A_1 and A_2 are piston areas at headside and rodside, as shown in Fig. 4.

Reversal of flow is obtained by an appropriate position motion of the spool, which is controlled by the input voltage to the valve. One common way to model this effect is through a resistive bridge, (Merritt, 1967). However, this results in complicated equations, and introduces additional numerical stiffness because two of the four resistances in the bridge are always very large. A method which yields the same results and is simpler to implement, is to assume that each actuation subsystem is driven with two pressure sources, P_{S1} and P_{S2} one of which is always set at pump pressure while the other is set at tank pressure. The spool position, and therefore the command input voltage, dictates which of the two sources is set to pump pressure. With this observation, the Linear Graph models introduced in (Papadopoulos et al, 1997), are modified to the ones depicted in Fig. 2 and 3.

c. Actuator Space Dynamics

Linear Graphs and similar systems methodologies are helpful in analysing and understanding dependencies in uni-dimensional multi-port energy domain systems. However, they are not well-suited in dealing with multidimensional coupled rigid-body dynamics. To address this problem, in this section link dynamics is rewritten as a set of scalar actuator-space equations, with state variables actuator displacements and speeds. This set also permits identifying terms with weak static or dynamic effects, a prerequisite for speeding up a simulation.

First, a detailed model for the rigid body dynamics of the manipulator in joint space coordinates is obtained including the swing, boom, and stick degrees-of-freedom. The equations were derived using Lagrangian dynamics. The rigid body equations have the form

$$\boldsymbol{M(q)}\cdot\ddot{\boldsymbol{q}} + \boldsymbol{V(q,\dot{q})} + \boldsymbol{G(q)} = \boldsymbol{\tau} = [\tau_{\mathrm{sw}}, \tau_{\mathrm{bm}}, \tau_{\mathrm{sk}}]^T \tag{3}$$

where $\boldsymbol{q} = [q_{\mathrm{sw}}, q_{\mathrm{bm}}, q_{\mathrm{sk}}]^T$ is the vector of joint angles, $\boldsymbol{M}(\boldsymbol{q})$ is a 3×3 mass matrix, $\boldsymbol{V}(\boldsymbol{q},\dot{\boldsymbol{q}})$ includes Coriolis and centrifugal terms, $\boldsymbol{G}(\boldsymbol{q})$ includes gravity terms, τ_{sw} is the torque provided by the hydraulic motor gearbox, and τ_{bm} and τ_{sk} are torques on the boom and stick joints generated by the hydraulic cylinders.

Next, the Jacobian $\boldsymbol{J}$ that relates joint angular speeds to actuator speeds

$$\dot{\boldsymbol{x}} = \boldsymbol{J}\cdot\dot{\boldsymbol{q}} \tag{4a}$$

also relates the net actuator forces acting on the manipulator links, $\boldsymbol{F}_{\mathrm{Net}}$, to torques in Eq. 3

$$\boldsymbol{\tau} = \boldsymbol{J}^T\cdot\boldsymbol{F}_{\mathrm{Net}} \tag{4b}$$

In Eq. 4, $\boldsymbol{x} = [q_{\mathrm{sw}}, x_{\mathrm{bm}}, x_{\mathrm{sk}}]^T$ is the vector of actuator displacements, x_{bm} and x_{sk} are the boom and stick cylinder displacements. The force $\boldsymbol{F}_{\mathrm{Net}}$ is related to the force or torque generated by the ideal hydraulic actuators, $\boldsymbol{F}_{\mathrm{Act}}$, as

$$\boldsymbol{F}_{\mathrm{Net}} = \boldsymbol{F}_{\mathrm{Act}} - \boldsymbol{B}\cdot\dot{\boldsymbol{x}} \tag{5}$$

where $\boldsymbol{F}_{\mathrm{Act}} = [\tau_{\mathrm{m}}, F_{\mathrm{bm}}, F_{\mathrm{sk}}]^T$ and τ_{m}, F_{bm} and F_{sk} are the swing motor, boom and stick ideal actuator torques or forces, and $\boldsymbol{B}$ is the associated damping. Since each link is independently actuated, $\boldsymbol{J}$ and $\boldsymbol{B}$ are diagonal, and furthermore, the first diagonal term of $\boldsymbol{J}$ is 1 since the swing actuator is rotational.

Using Eq. 4a, the joint angular acceleration is expressed as

$$\ddot{\boldsymbol{q}} = \dot{\boldsymbol{J}}^{-1}\dot{\boldsymbol{x}} + \boldsymbol{J}^{-1}\ddot{\boldsymbol{x}} \tag{6}$$

Also, the mass matrix $\boldsymbol{M}(\boldsymbol{q})$ is decomposed to its diagonal terms $\boldsymbol{M}_{\mathrm{D}}$ and its off-diagonal terms $\boldsymbol{M}_{\mathrm{OD}}$

$$\boldsymbol{M}_{\mathrm{D}} = diag(\boldsymbol{M}(\boldsymbol{q})) \tag{7a}$$

$$\boldsymbol{M}_{\mathrm{OD}} = \boldsymbol{M}(\boldsymbol{q}) - diag(\boldsymbol{M}(\boldsymbol{q})) \tag{7b}$$

and therefore

$$\boldsymbol{M}(\boldsymbol{q}) = \boldsymbol{M}_{\mathrm{D}} + \boldsymbol{M}_{\mathrm{OD}} \tag{8}$$

Using Eq. 4-8, Eq. 3 can now be expressed in actuator space coordinates as

$$\boldsymbol{M}_{\mathrm{Eq}}\ddot{\boldsymbol{x}} + \boldsymbol{B}\dot{\boldsymbol{x}} + \boldsymbol{F}_{\mathrm{S}} = \boldsymbol{F}_{\mathrm{Act}} \tag{9}$$

where

$$\boldsymbol{M}_{\mathrm{Eq}} = \boldsymbol{J}^{-T}\boldsymbol{M}_{\mathrm{D}}\boldsymbol{J}^{-1} \tag{10}$$

$$\boldsymbol{F}_{\mathrm{S}} = \boldsymbol{J}^{-T}[\boldsymbol{M}_{\mathrm{OD}}\boldsymbol{J}^{-1}\ddot{\boldsymbol{x}} + \boldsymbol{M}(\boldsymbol{q})\dot{\boldsymbol{J}}^{-1}\dot{\boldsymbol{x}} + \boldsymbol{V}(\boldsymbol{q},\dot{\boldsymbol{q}}) + \boldsymbol{G}(\boldsymbol{q})] \tag{11}$$

Because both $\boldsymbol{M}_{\mathrm{D}}$ and $\boldsymbol{J}$ are diagonal matrices, $\boldsymbol{M}_{\mathrm{Eq}}$ is also diagonal, and $\dot{\boldsymbol{J}}^{-1}$ is simple and available analytically.

The continuity equations, i.e. force balance equations, at the nodes $\dot{q}_{\mathrm{sw}}$ and $\dot{x}_{\mathrm{p}}$ in Fig. 2 and 3 can be written as

Node $\dot{q}_{\mathrm{sw}}$:

$$J_{\mathrm{Eq}}\ddot{q}_{\mathrm{sw}} + B_{\mathrm{m}}\,\dot{q}_{\mathrm{sw}} + T_{\mathrm{S}} = N\,D_{\mathrm{m}}\,P_1 = \tau_{\mathrm{m}} = \tau_{\mathrm{sw}} \tag{12a}$$

Node $\dot{x}_{\mathrm{p}}$:

$$M_{\mathrm{Eq}}\,\ddot{x}_{\mathrm{p}} + B_{\mathrm{p}}\,\dot{x}_{\mathrm{p}} + F_{\mathrm{S}} = A_1\,P_1 - A_2\,P_4 = F_{\mathrm{p}} \tag{12b}$$

where again *p* stands for *bm* (boom) or *sk* (stick). Eq. 12a basically states that the motor torque is proportional to the motor pressure drop P_1, see Eq. 1 and that it accelerates the motor and gearbox inertia, overcomes the motor viscous friction, and supplies the manipulator with some torque. Similarly, Eq. 12b is a force balance for the boom or stick pistons.

Direct comparison between Eq. 9 and 12 shows that the equivalent configuration dependent mass-/inertia in the Linear Graphs of Fig. 2 and 3 are the diagonal elements of $\boldsymbol{M}_{\mathrm{Eq}}$ and that the force/torque sources are the elements of $\boldsymbol{F}_{\mathrm{S}}$. Eq. 12 provide a direct interface of hydraulic system modelling and actuator space dynamics, allowing model simplifications, and yield better understanding of link-actuator dynamics at systems level.

With the above modifications a set of eighteen first-order nonlinear differential equations result, twelve for the actuation subsystem and six for the manipulator modelling. The detailed equations are given in Appendix A. Three PID link controllers were implemented both as part of the experimental machine and the simulator software. The controllers input commands are joint positions necessary to obtain coordinated motion of the manipulator endpoint, while their outputs are voltages driving valve spools and therefore modulating orifice resistances. This modulation and its associated numerical problems are addressed in the next section.

3 Valve Closure Stiffness

Valve orifices are modelled as non-linear fluid resistances according to

$$P = C_{\mathrm{R}} \cdot Q^2 \mathrm{sign}(Q) \tag{13}$$

where Q is the flow through the orifice and P its across pressure drop. A polynomial fitted to experimental data is used to find the orifice resistance C_{R} as a function of the input voltage sent to the valve, see (Papadopoulos et al, 1997).

When an overlapped valve closes, the flow through it ceases, and its orifice resistance becomes infinite. Since infinite numbers are impossible in simulation, a very large value, referred to as the *maximum-resistance* at valve closure, must be chosen instead. As a result, residual flows leaking through the orifices appear in simulation when a valve is closed, leading to a simulator non-realistic drift of the manipulator links. In addition, as the control voltage changes sign and the valve opens again, this residual flow changes direction abruptly due to the associated change in pressure source conditions. This effect creates undesirable discontinuities in the fluid flow variables of the actuation system. As a result, numerical integration at these instances becomes computationally intensive and sometimes even impossible, depending on the choice of integration method and the magnitude of tolerated errors. In such instances, the realism that a simulator must achieve is seriously affected.

To tackle this problem, a new set of "closed-valve" equations is introduced to describe system behaviour during valve closure, and the system is described by one set of equations when the valve is open, and by another set when the valve closes.

In these new closed-valve models, elements that play no role due to valve closure, i.e. valve resistances and pressure sources, are removed. Since no flow is present when the valve is closed, the inertances are also removed. The fluid capacitance elements are maintained because hose and fluid capacitive behaviour is present. On the mechanical side, a link may oscillate at very low amplitudes due to fluid and line compressibility, but it will not drift.

Simulating valve closure with model switching requires continuity in the state variables; or the numerical integrator may fail. However, since at the verge of

simulated valve opening there is some residual flow due to the finite maximum resistance, while there is zero flow when the valve is closed, there is a need for an additional mechanism to maintain continuity. Note that the residual flow resulting when the valve is about to open (or before closing) is not constant, but it depends on the pressure difference across the valve, a quantity that varies with time, see also Eq. 13. Also note that although removal of the inertial elements simplifies the system dynamics and speeds up integration, it also removes associated flow rate state variables.

To address these issues, first the residual flow at the verge of opening or closing a valve is computed as a function of the pressure difference between the source and the line pressure, $P_{S,i} - P_{C,i}$. Indeed, using simple Linear Graph compatibility (pressure) equations, and the fact that a zero rate of flow rates corresponds to a zero pressure drop across an inertance (Rowell and Wormley, 1997), one can show that this residual flow is given by

$$Q_{res,i} = \sqrt{\left|P_{S,i} - P_{C,i}\right| / C_{R,i}} \cdot \mathrm{sign}\left(P_{S,i} - P_{C,i}\right) \qquad (14)$$

Once the valve is closed, and the dynamic equations are switched to the closed valve model, there is a need for a state variable which will quickly reach (or track) the value given by Eq. 14. This is achieved by a simple first order system whose input is $Q_{res,i}$

$$\frac{dQ_{I,i}}{dt} + \frac{1}{\tau_Q}\left(Q_{I,i} - Q_{res,i}\right) = 0 \qquad (15)$$

where τ_Q is a time constant that must be chosen reasonably small, and $Q_{I,i}$ is the flow through the valve orifice and the inertance element I_i. It was found that a reasonable value is τ_Q = 0.01 s. Eq. 14 and 15 eliminate all flow discontinuities encountered during valve switching, and hence they increase simulation performance.

Figure 5 shows the simulated tracking error response due to some stick motion, in comparison to the experimental one. As shown in the figure, the model still predicts accurately the oscillations caused by the hydraulic dynamics in the fluid lines, see for example the oscillations at 8 s, 30 s, etc. However, integration of the dual model equations is not slowed down during valve switchings and integration can proceed fast without numerical problems.

On the other hand, because these line oscillations occur at relatively high frequencies (around 20 Hz) the integrator slows down when these occur. These oscillations are secondary effects that are filtered by the mechanical rigid-body dynamics that is much slower than its hydraulic counterpart. Since the purpose of the simulator is to display the manipulator motion, these fast dynamic effects are of no interest here and can be eliminated.

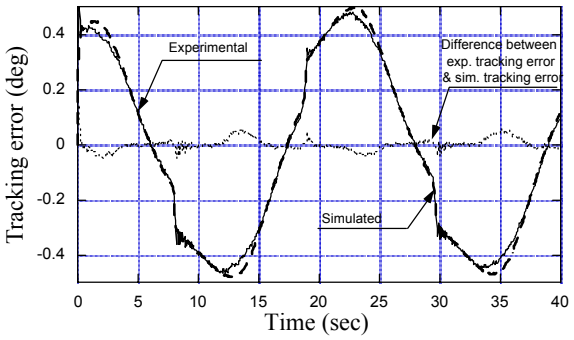

Fig. 5: *Comparison of stick tracking errors*

In the next section, a new set of actuator models is proposed in which hydraulic dynamic elements are removed for further speed improvements.

4 Reduced Actuator Systems

Experimental and simulation results confirmed that the rigid body dynamics act as low-pass filters, filtering the oscillations inherent to the hydraulic actuation to a negligible level as far as the simulator is concerned. Hence, it was concluded that the removal of the hydraulic dynamics would not reduce the required accuracy significantly. Therefore, the reduced hydraulic actuation systems were modelled simply as resistive networks, see Fig. 6 and 7. These "reduced" models have only six state variables compared to eighteen of the "full" models described in the previous section.

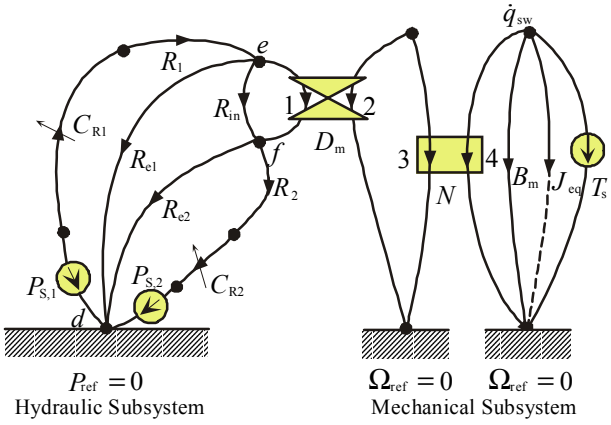

Fig. 6: *The swing actuator reduced model*

To deal with numerical stiffness problems associated with a closing valve, the approach taken in Section 3 is followed here, and hence, two models for each actuator subsystem are developed: one for the interval at which the valve is open, and for the interval at which the valve is closed. The open valve models are shown in Fig. 6 and 7, while in the closed valve models, the pressure sources and the valve orifice resistances are removed. Again, because no infinite maximum resistance values can be used at valve clo-

sure, there are small discontinuities in flows through the valves during model switching. Here, due to the structure of the reduced models, a discontinuity in residual flows directly becomes a discontinuity in the joint actuator velocities, see Eq. 1, and 2. To prevent these discontinuities, first order differential equations were used as explained in Section 3.

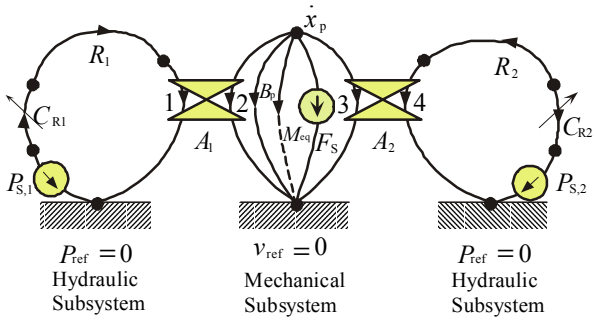

Fig. 7: *The cylinder actuator reduced model*

In order to find the residual flows through the valves, an inverse dynamics procedure is employed. If a joint is locked and does not move, the corresponding valve is closed. However, the joint actuator applies a force or torque to keep the joint from moving. This force or torque and the corresponding load pressure can be computed knowing the state of the manipulator, i.e. the motion of its links and the gravity loads. This is an inverse dynamics procedure. In simulation, a closed valve is represented by a large but not infinite resistance. Therefore, the valve pressure drop required to maintain the load pressure at the actuator when the valve is almost closed (or almost open) results in a residual flow and a corresponding residual velocity at the mechanical side.

In more detail, it is assumed that when a valve closes, the corresponding joint's angular accelerations are zero. Also, the residual flow through the lines is very small, resulting in very small angular velocities, and therefore velocity and damping terms can be neglected. Hence, when the valve of a cylinder or motor closes, velocity and acceleration terms vanish and Eq. 12 become

Node $\dot{q}_{sw}$:

$$T_S = N\, D_m\, P_1 = \tau_{sw} \tag{16a}$$

Node $\dot{x}_p$:

$$F_S = A_1\, P_1 - A_2\, P_4 = F_p \tag{16b}$$

The force or torque source elements F_S or T_S can be determined using Eq. 11. In the case of a swing motor, Eq. 16a yields an expression for P_1. However, to compute the pressures P_{Re1} and P_{Re2}, a Newton-Raphson-based numerical solver must be employed because of the existence of algebraic loops. Computation of these two pressures allows one to find the pressure drops across the valve, and subsequently to compute the residual flows.

In the case of a piston type actuator, the piston velocity $\dot{x}_p$ can be written as a function of F_S using the elemental, continuity and compatibility equations defined by the Linear Graph methodology. Since the effect of piston damping is small compared to the damping due to valve resistance at valve closure, piston damping is neglected, and the residual piston velocity results as a simple function of F_S.

$$\dot{x}_p = \sqrt{\frac{\left|A_1 P_{S1} - A_2 P_{S2} - F_S\right|}{(C_{R1} + R_1)A_1^3 + (C_{R2} + R_2)A_2^3}} \cdot \text{sign}(A_1 P_{S1} - A_2 P_{S2} - F_S) \tag{17}$$

The residual flows through the valve are then given as the product of the appropriate piston area by $\dot{x}_p$.

Next, in the interest of comparing the full model response to that of the reduced one, expressions are developed to calculate the pressures at the inlet and outlet of the hydraulic actuators, i.e. pressures P_1 and P_4 for the cylinders, see Fig. 4 and 7, and pressures P_{Re1} and P_{Re2} for the hydraulic motor, see Fig. 6. In particular, pressures P_{Re1} and P_{Re2} are the ones across nodes e-d and f-d in Fig. 6.

In the case of the open-valve models, these pressures can be determined using continuity and compatibility equations, as they are simple algebraic functions of the state variables. However, the pressures P_{Re1} and P_{Re2} associated with the hydraulic motor are determined after solving the algebraic loops encountered due to the leakage resistive elements R_{e1} and R_{e2}.

In the case of the closed-valve models, the motor pressures P_{Re1} and P_{Re2} are again found by solving iteratively the algebraic loops. However, the pressures P_1 and P_4 of the hydraulic cylinders cannot be found separately, because the inverse dynamics procedure yields the force applied by the actuator, but not the individual pressures on each side of the piston, see Eq. 12b. This is because the headside and rodside piston areas are unequal due to the existence of the rod, see Fig. 4. Therefore, to compute the individual pressures, more information is needed. This information can be obtained using the observation that individual piston chamber pressures settle to a level, which is related to compressibility and capacitive effects of the lines and the oil.

To this end, the full model described by the linear graph of Fig. 3 is examined with focus on the action of the capacitive elements when a valve is closed. The elemental equation of the first fluid capacitance is, (Rowell and Wormley, 1997)

$$\frac{dP_{C1}}{dt} = \frac{1}{C_1} Q_{C1} \tag{18}$$

where C_1 is the element fluid capacitance, $P_{C1}$is the pressure drop across the element, and Q_{C1} is the flow

through it. The Q_{C1}flow is related to piston velocity, see Eq. 2, as

$$Q_{C1} = -Q_1 = -A_1 v_{M,Eq} = -A_1 \dot{x}_p \tag{19}$$

Replacing Eq. 19 into Eq. 18, and integrating Eq. 19 from an initial state *i* to a current one, the pressure across C_1 is expressed as a function of the piston position x_p

$$P_{C1} = P_{C1,i} - \frac{A_1}{C_1}\left(x_p - x_{p,i}\right) \tag{20}$$

where $P_{C1,i}$ and $x_{p,i}$ are respectively, the pressure drop across the capacitance C_1, and the piston position at a given initial state *i*. A similar expression can be found for the second capacitance C_2. Using these expressions into Eq. 12b and expressing all the variables in terms of the piston position x_p, the differential equation becomes

$$M_{Eq}\ddot{x}_p + B_{Eq}\dot{x}_p + K_{Eq}\left(x_p - x_{p,i}\right) = F_{S,i} - F_S \tag{21}$$

where

$$B_{Eq} = \left(R_1 A_1^3 + R_2 A_2^3\right)\cdot\left|\dot{x}_p\right| + B_p \tag{22}$$

$$K_{Eq} = \frac{A_1^2}{C_1} + \frac{A_2^2}{C_2} \tag{23}$$

$$F_{S,i} = A_1 P_{C1,i} - A_2 P_{C2,i} \tag{24}$$

and B_{Eq} is the equivalent damping, B_p is the piston damping, where R_1 and R_2 are the fluid line non-linear resistance constants, defined by an equation similar to Eq. 13, $x_{p,i}$ is the position of the piston at state *i*, and K_{Eq} is an equivalent spring constant.

When a valve is closed, the acceleration and velocity of a cylinder's piston quickly become negligible. Therefore, setting the derivatives of x_p equal to zero, Eq. 21 allows one to compute the position of the piston as

$$x_p = x_{p,i} + \left(F_{S,i} - F_S\right)/K_{Eq} \tag{25}$$

Also, since the piston is not moving, there is no flow through the fluid lines, and therefore the pressure drop across the resistive elements R_1 and R_2 is zero. As a result, the compatibility equations require that pressures P_1 and P_4 be equal to the pressures across the capacitive elements C_1 and C_2, P_{C1} and P_{C2}, respectively.

Combining the results above, the pressures at the inlet and outlet of the piston actuators when the valve is closed are given by the following expressions

$$P_1 = P_{1,i} - \frac{A_1}{C_1}\cdot\frac{F_{S,i} - F_S}{K_{Eq}} \tag{26a}$$

$$P_4 = P_{4,i} + \frac{A_1}{C_1}\cdot\frac{F_{S,i} - F_S}{K_{Eq}} \tag{26b}$$

where $P_{1,i}$ and $P_{4,i}$ are the lower and upper piston pressures at some initial state *i*. For simulation purposes, this initial state is chosen to be the time at which a valve closes, when P_1 and P_4 are known.

5 Implementation Results

The full model simulation results presented in (Papadopoulos et al, 1997) were in excellent agreement with the experimental results, thus validating the full model, see also Fig. 5. Here, the full model response, (solid thin line), is compared to the response of the reduced model, (dashed thick line), while the stick is commanded to follow a sinusoidal trajectory. The same controller has been used in all cases, both in structure and gain values.

Figure 8 shows a comparison of the stick joint position errors for the two models, Fig. 9 a comparison of the stick cylinder output pressure (P_4), and Fig. 10 the command voltage sent to the stick's valve, responsible for the responses in Fig. 8 and 9, during a stick sinusoidal motion.

As shown in Fig. 8, the stick tracking error response that results from the full and the reduced models are in excellent agreement, except where the full model predicts hydraulic oscillations. This is expected, since the reduced model does not include line or oil dynamics. However, as explained earlier, this is not required for a real-time graphical simulator.

The same behaviour is observed in Fig. 9, where the stick output pressure is plotted. The two model responses differ slightly where the full model predicts hydraulic oscillations.

Figure 10 shows that the controller command voltages to the valves are identical for the two models. This is due to the fact that small pressure oscillations are not observed in stick angular positions due to mechanical filtering, and therefore, the controller command voltages that depend on sensed and desired angular positions are identical.

Boom cylinder pressure predicted by the closed-valve reduced model was compared to the same pressure given by the closed-valve full model, while the stick was commanded to follow the same sinusoidal trajectory as before and the boom valve was closed, see Fig. 11. This figure shows that as expected, piston chamber pressures for pistons that are locked in position vary during motions of the manipulator, as expected.

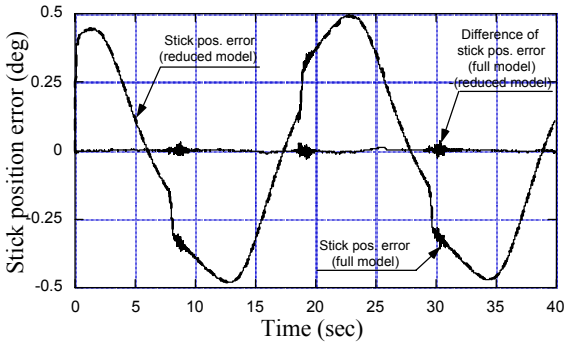

Fig. 8: *Stick position tracking error*

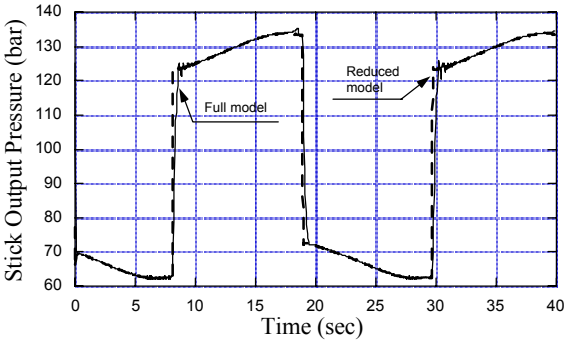

Fig. 9: *Stick cylinder output pressure*

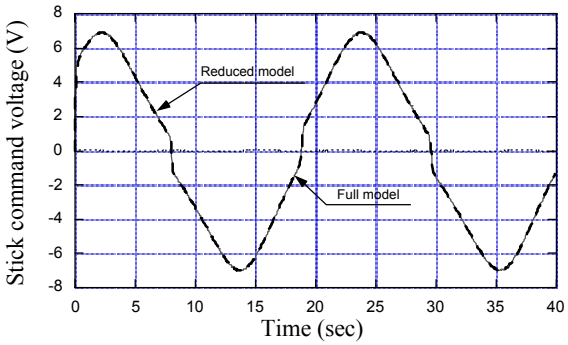

Fig. 10: *Stick command voltage*

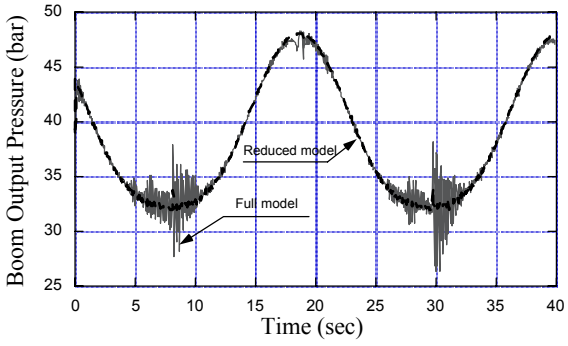

Fig. 11: *Boom cylinder output pressure*

The obtained simulation results show that the reduced model accurately predicts the response of the electro-hydraulically actuated manipulator, while it eliminates the small oscillations caused by the hydraulic dynamics. As mentioned previously, for the purpose of a real time graphical simulation, these oscillations are not required since the motions they induce are not visible. On the other hand, the removal of these oscillations significantly decreases the number of computations required to predict the behaviour of the system.

For the above simulation results, a relatively high maximum-resistance approximation for the valve closing point was used. The continuity of states and reduced models for all three actuators were implemented. The simulation was run on a 150 MHz, R4400 processor Silicon Graphics Extreme workstation and Matlab/Simulink was used. The running time was reduced by a factor of 3.5, from 28 min down to 8 min for a 40 s simulation. By compiling the reduced models, and relaxing the valve maximum-resistance value, the running time was reduced to 47 s, i.e., by a factor of 35.

The simulation time can be reduced further by fine tuning the code and compiling it as a stand-alone package. Also, although the simulator engine currently runs on a SGI workstation, it can also run on standard PC computers with OpenGL libraries, equipped with relatively inexpensive fast processors and graphics cards. Therefore, realistic real-time simulation of an electro-hydraulic system is achievable.

6 Conclusions

This paper focused on the development of a real-time graphical simulator engine for forestry machines. The rigid body dynamics of a machine's manipulator was integrated with electrohydraulic actuator models and joint controllers were added. Stiffness and discontinuity problems related to valve closure/opening were described and solutions proposed. To accelerate simulation running time, a reduced model of the actuators was introduced. The fluid line dynamics was eliminated and the hydraulic actuation system was modelled as a purely resistive network. Full and reduced models were compared and it was found that the reduced model properly represents the required effects. In addition, the running time using the reduced model simulation increased by a factor of 35 without sacrificing response accuracy.

Nomenclature

A	piston area	[m^2]
B	linear damping	[Ns/m]
C	fluid capacitance	[m^4s^2/kg]
C_R	resistance coefficient	[m]
D_m	hydraulic motor constant	[m^3/rad]
F	force	[N]
$\boldsymbol{F}_S$	force coupling terms	[N]
I	fluid line inertance	[kg/m^4]

$\boldsymbol{J}$	Jacobian matrix	
K	spring constant	[N/m]
$\boldsymbol{M}$	mass matrix	
N	swing gearbox ratio	-
P	pressure	[N/m^2]
P_i	pressure across graph element i	[N/m^2]
Q	flow rate	[m^3/s]
$Q_{res,i}$	residual flow rate	[m^3/s]
$\boldsymbol{q}$	joint angles	
R	fluid line resistance	[kg/m^{4}s]
$\boldsymbol{\tau}$	torque / force vector	
τ, T	torque	[Nm]
τ_Q	time constant	[s]
v	linear velocity	[m/s]
x	linear displacement	[m]
Ω	angular velocity	[rad/s]

Indices

bm	as an index indicates boom
Eq	as an index indicates equivalent
p	as an index indicates piston
s	as an index indicates source
sk	as an index indicates stick
sw	as an index indicates swing

Acknowledgements

The financial support for this work by the Ministère de l'Industrie, du Commerce, de la Science et de la Technologie of Quebec, (MICST) under the program SYNERGIE, is gratefully acknowledged. Also, the authors wish to thank P. Freedman (CRIM), I. Makkonen (FERIC), R. Germain and J. LeBrun (Denharco), D. Éthier, and R. Lessard (Autolog), and S. Sarkar, B. Mu, and R. Frenette (McGill University) for their assistance in various aspects of this work.

References

Choi, S. K. and **Yuh, J.** 2001. A Virtual Collaborative World Simulator for Underwater Robots Using Multi-dimensional, Synthetic Environment, *Proc. IEEE Int. Conf. on Robotics and Automation*, Seoul, Korea, pp. 926-931.

Courteau, J. 1994. Robotics in Canadian Forestry, *IEEE Canadian Review*, pp. 10-13.

Freedman, P. 1999. 3D Training Simulators for the Forestry Industry, *Proc. Canadian Woodlands Forum 80th Annual Meeting*, Thunder Bay, Ontario, Canada, April 21-24.

Freedman, P. MacKenzie, P., and **J.-F. Lapointe, A.** 1997. Computer-Based Training Environment for Forestry Telemanipulation, *Proc. of the 1997 International Conference on Intelligent Robots and Systems (IROS '97)*, September 8-12, Grenoble, France.

Freedman, P., Papadopoulos, E., Poussart, D., Gosselin, C., and **Courteau, J.** 1995. ATREF: Application des Technologies Robotiques aux Équipements Forestiers, *Proc. 1995 Canadian Conf. on Electrical and Computer Engineering*, Montreal, PQ, Canada, Sept. 5-8.

Lawrence, P. D. et al. 1993. Computer-Assisted Control of Excavator-Based Machines, *SAE Technical Paper* # 932486, Warrendale, PA, 1993.

Merritt, H. E. 1967. *Hydraulic Control Systems*. John Wiley & Sons.

Mort, P. et al. 1997. Interactive Training Simulator for a Pipe Diversion Task in the Nuclear Industry, *Proc. IEEE Int. Conf. on Robotics and Automation*, Albuquerque, NM, pp. 1324-1330.

Papadopoulos, E. and **Sarkar, S.** 1997. The Dynamics of an Articulated Forestry Machine and its Applications, *Proc. IEEE Int. Conf. on Robotics and Automation*, Albuquerque, NM.

Papadopoulos, E., Mu, B., and **Frenette, R.** 1997. Modelling and Identification of an Electrohydraulic Articulated Forestry Machine, *Proc. IEEE Int. Conf. on Robotics and Automation*, Albuquerque, NM, pp. 60-65.

Piedboeuf, J. C., et al. 1999. Task Verification Facility for the Canadian Special Purpose Dextrous Manipulator, *Proc. IEEE Int. Conf. on Robotics and Automation*, Detroit, MI, pp. 1077-1083.

Rosenberg, R. and **Karnopp, D.** 1983. *Introduction to Physical System Dynamics*, McGraw Hill, New York, NY.

Rowell, D. and **Wormley, D.** 1997. *System Dynamics*, Prentice Hall.

Ruspini, D. and **Khatib, O.** 2000. *Proc. International Conference on Intelligent Robots and Systems (IROS '00)*, Nov. 01-03, Takamatsu, Japan.

Yoneda, M. et al. 1997. Assistance System for Crane Operation using Multimodal Display, *Proc. IEEE Int. Conf. on Robotics and Automation*, Albuquerque, NM, pp. 40-46.

Appendix A

The equations of motion for the rigid body manipulator, were derived separately in the joint space of the manipulator using a Lagrangian approach. These have the form (Papadopoulos and Sarkar, 1997)

$$\boldsymbol{M}(\boldsymbol{q})\cdot\ddot{\boldsymbol{q}}+\boldsymbol{V}(\boldsymbol{q},\dot{\boldsymbol{q}})+\boldsymbol{G}(\boldsymbol{q})=\boldsymbol{\tau} \tag{A1}$$

where $\boldsymbol{q} = [q_{\mathrm{sw}}, q_{\mathrm{bm}}, q_{\mathrm{sk}}]^T$ is the vector of manipulator *joint angles*, $\boldsymbol{M}(\boldsymbol{q})$ is a mass matrix, $\mathbf{V(q,\dot{q})}$ includes Coriolis and centrifugal terms, $\mathbf{G(q)}$ includes gravity terms, and $\boldsymbol{\tau}$ is the input torque provided by the actuators. To integrate this model to the hydraulic actuator models, one needs to provide expressions transforming pressure differences to forces or torques, and angular velocities to flows.

For the actuators, Eq. 4 is repeated here

$$\dot{\boldsymbol{x}}=\boldsymbol{J}\,\dot{\boldsymbol{q}},\ \ \boldsymbol{\tau}=\boldsymbol{J}^T\cdot\left(\boldsymbol{F}_{\mathrm{Act}}-\boldsymbol{B}\cdot\dot{\boldsymbol{x}}\right) \tag{A2}$$

where $\boldsymbol{x} = [q_{\mathrm{sw}}, x_{\mathrm{bm}}, x_{\mathrm{sk}}]^T$ is the vector of *actuator displacements*, x_{bm} and x_{sk} are the boom and stick cylinder displacements, $\boldsymbol{F}_{\mathrm{Act}} = [\tau_{\mathrm{m}}, F_{\mathrm{bm}}, F_{\mathrm{sk}}]^T$ and τ_{m}, F_{bm} and F_{sk} are the swing motor, boom and stick ideal actuator torques or forces, and $\boldsymbol{B}$ is the associated damping. Since each link is independently actuated, the Jacobian $\boldsymbol{J}$ is a diagonal matrix.

For single-ended type of cylinders, we have

$$\begin{bmatrix}F_{\mathrm{bm}}\\F_{\mathrm{sk}}\end{bmatrix}=\begin{bmatrix}A_{1\_\mathrm{bm}} & -A_{2\_\mathrm{bm}} & 0 & 0\\ 0 & 0 & A_{1\_\mathrm{sk}} & -A_{2\_\mathrm{sk}}\end{bmatrix}\begin{bmatrix}P_{1\_\mathrm{bm}}\\P_{4\_\mathrm{bm}}\\P_{1\_\mathrm{sk}}\\P_{4\_\mathrm{sk}}\end{bmatrix} \tag{A3a}$$

$$\begin{bmatrix}Q_{1\_\mathrm{bm}}\\Q_{1\_\mathrm{sk}}\\Q_{4\_\mathrm{bm}}\\Q_{4\_\mathrm{sk}}\end{bmatrix}=-\begin{bmatrix}A_{1\_\mathrm{bm}} & 0\\ 0 & A_{1\_\mathrm{sk}}\\ A_{2\_\mathrm{bm}} & 0\\ 0 & A_{2\_\mathrm{sk}}\end{bmatrix}\begin{bmatrix}\dot{x}_{\mathrm{bm}}\\\dot{x}_{\mathrm{sk}}\end{bmatrix} \tag{A3b}$$

where A_{1_bm}, A_{2_bm}, A_{1_sk}, A_{2_sk} are driving and returning areas of the boom and stick pistons; F_{bm}, F_{sk} are the forces generated by boom and stick cylinders. Similarly, P_{1_bm}, P_{4_bm}, P_{1_sk}, P_{4_sk} are pressures at inlet and outlet of the boom and stick cylinders, and Q_{1_bm}, Q_{4_bm}, Q_{1_sk}, Q_{4_sk} are flow rates. The negative sign in the second equation is due to Linear Graph conventions. Therefore, the transduction equations can be written as

$$\begin{aligned}\begin{bmatrix}\tau_{\mathrm{bm}}\\\tau_{\mathrm{sk}}\end{bmatrix}&=\boldsymbol{\tau}_{\mathrm{cyl}}=\boldsymbol{J}^T(\boldsymbol{q})\cdot\boldsymbol{F}=\boldsymbol{J}^T(\boldsymbol{q})\cdot\begin{bmatrix}F_{\mathrm{bm}}\\F_{\mathrm{sk}}\end{bmatrix}\\&=\boldsymbol{J}^T\begin{bmatrix}A_{1\_\mathrm{bm}} & -A_{2\_\mathrm{bm}} & 0 & 0\\ 0 & 0 & A_{1\_\mathrm{sk}} & -A_{2\_\mathrm{sk}}\end{bmatrix}\begin{bmatrix}P_{1\_\mathrm{bm}}\\P_{4\_\mathrm{bm}}\\P_{1\_\mathrm{sk}}\\P_{4\_\mathrm{sk}}\end{bmatrix}\end{aligned} \tag{A4a}$$

$$\begin{aligned}\begin{pmatrix}\dot{q}_{\mathrm{bm}}\\\dot{q}_{\mathrm{sk}}\end{pmatrix}&=\boldsymbol{J}^{-1}\begin{bmatrix}\dot{x}_{\mathrm{bm}}\\\dot{x}_{\mathrm{sk}}\end{bmatrix}=\\&=-\boldsymbol{J}^{-1}\begin{bmatrix}1/A_{1\_\mathrm{bm}} & 0\\ 0 & 1/A_{1\_\mathrm{sk}}\end{bmatrix}\begin{bmatrix}Q_{1\_\mathrm{bm}}\\Q_{4\_\mathrm{sk}}\end{bmatrix}\\&=-\boldsymbol{J}^{-1}\begin{bmatrix}1/A_{2\_\mathrm{bm}} & 0\\ 0 & 1/A_{2\_\mathrm{sk}}\end{bmatrix}\begin{bmatrix}Q_{1\_\mathrm{bm}}\\Q_{4\_\mathrm{sk}}\end{bmatrix}\end{aligned} \tag{A4b}$$

The transduction equation for the swing motor is more standard, and including the gear train results in

$$\begin{bmatrix}\dot{q}_{\mathrm{sw}}\\\tau_{\mathrm{sw}}\end{bmatrix}=\begin{bmatrix}0 & 1/(D_{\mathrm{m}}N)\\ -D_{\mathrm{m}}N & 0\end{bmatrix}\begin{bmatrix}P_{1\_\mathrm{sw}}\\Q_{1\_\mathrm{sw}}\end{bmatrix} \tag{A5}$$

The relationship between manipulator dynamics, in terms of variables $\boldsymbol{\tau}$ and $\dot{\mathbf{q}}$ and electrohydraulic actuator dynamics, in terms of variables $\boldsymbol{P}$, $\boldsymbol{Q}$ are set up. The overall dynamic equations for the three dof manipulator are given below.

$$\begin{aligned}
&\dot{\boldsymbol{q}}_1=\boldsymbol{q}_2\\
&\dot{\boldsymbol{q}}_2=\boldsymbol{M}(\boldsymbol{q}_1)^{-1}\left\{-\boldsymbol{V}(\boldsymbol{q}_1,\boldsymbol{q}_2)-\boldsymbol{G}(\boldsymbol{q}_1)+\boldsymbol{\tau}\right\}\\
&\dot{P}_{\mathrm{C1_sw}}=\left(Q_{\mathrm{i,1_sw}}-\left(P_{\mathrm{C1_sw}}-P_{\mathrm{Rin}}(\dot{q}_{\mathrm{sw}})-P_{\mathrm{R2}}-P_{\mathrm{C2_sw}}\right)/R_1\right)/C_{1_\mathrm{sw}}\\
&\dot{P}_{\mathrm{C2_sw}}=\{\left(P_{\mathrm{C1_sw}}-P_{\mathrm{R_{in}}}(\dot{q}_{\mathrm{sw}})-P_{\mathrm{R2}}-P_{\mathrm{C2_sw}}\right)R_1-\\
&-\left(P_{\mathrm{Rin}}(\dot{q}_{\mathrm{sw}})+P_{\mathrm{R2}}+P_{\mathrm{C2_sw}}\right)/R_{\mathrm{e1}}\\
&-\left(P_{\mathrm{C2_sw}}+P_{\mathrm{R2}}\right)/R_{\mathrm{e2}}-Q_{\mathrm{i,2_sw}}\}/C_{2_\mathrm{sw}}\\
&\dot{Q}_{\mathrm{i,1_sw}}=\left(P_{\mathrm{S,1_sw}}-C_{\mathrm{R}}\cdot Q_{\mathrm{i,1_sw}}{}^2\cdot\mathrm{sign}\left(Q_{\mathrm{i,1_sw}}\right)-P_{\mathrm{C1_sw}}\right)/I_{1_\mathrm{sw}}\\
&\dot{Q}_{\mathrm{i,2_sw}}=\left(P_{\mathrm{S,2_sw}}+P_{\mathrm{C2_sw}}-C_{\mathrm{R'}}\cdot Q_{\mathrm{i,2_sw}}{}^2\cdot\mathrm{sign}\left(Q_{\mathrm{i,2_sw}}\right)\right)/I_{2_\mathrm{sw}}\\
&\dot{P}_{\mathrm{C1_bm}}=\left(Q_{\mathrm{i,1_bm}}-A_{1_\mathrm{bm}}\cdot\dot{x}_{\mathrm{bm}}\right)/C_{1_\mathrm{bm}}\\
&\dot{P}_{\mathrm{C2_bm}}=\left(A_{2_\mathrm{bm}}\cdot\dot{x}_{\mathrm{bm}}-Q_{\mathrm{i,2_bm}}\right)/C_{2_\mathrm{bm}}\\
&\dot{Q}_{\mathrm{i,1_bm}}=\left(P_{\mathrm{S,1_bm}}-C_{\mathrm{R}}\cdot Q_{\mathrm{i,1_bm}}{}^2\cdot\mathrm{sign}\left(Q_{\mathrm{i,1_bm}}\right)-P_{\mathrm{C1_bm}}\right)/I_{1_\mathrm{bm}}\\
&\dot{Q}_{\mathrm{i,2_bm}}=\left(P_{\mathrm{S,2_bm}}+P_{\mathrm{C2_bm}}-C_{\mathrm{R'}}\cdot Q_{\mathrm{i,2_bm}}{}^2\cdot\mathrm{sign}\left(Q_{\mathrm{i,2_bm}}\right)\right)/I_{2_\mathrm{bm}}\\
&\dot{P}_{\mathrm{C1_sk}}=\left(Q_{\mathrm{i,1_sk}}-A_{1_\mathrm{sk}}\cdot\dot{x}_{\mathrm{sk}}\right)/C_{1_\mathrm{sk}}\\
&\dot{P}_{\mathrm{C2_sk}}=\left(A_{2_\mathrm{sk}}\cdot\dot{x}_{\mathrm{sk}}-Q_{\mathrm{i,2_sk}}\right)/C_{2_\mathrm{sk}}\\
&\dot{Q}_{\mathrm{i,1_sk}}=\left(P_{\mathrm{S,1_sk}}-C_{\mathrm{R}}\cdot Q_{\mathrm{i,1_sk}}{}^2\cdot\mathrm{sign}\left(Q_{\mathrm{i,1_sk}}\right)-P_{\mathrm{C1_sk}}\right)/I_{1_\mathrm{sk}}\\
&\dot{Q}_{\mathrm{i,2_sk}}=\left(P_{\mathrm{S,2_sk}}+P_{\mathrm{C2_sk}}-C_{\mathrm{R'}}\cdot Q_{\mathrm{i,2_sk}}{}^2\cdot\mathrm{sign}\left(Q_{\mathrm{i,2_sk}}\right)\right)/I_{2_\mathrm{sk}}
\end{aligned} \tag{A6a}$$

where

$$\boldsymbol{q}_1=\boldsymbol{q}=\begin{bmatrix}q_{\mathrm{sw}} & q_{\mathrm{bm}} & q_{\mathrm{sk}}\end{bmatrix}^T \tag{A6b}$$

Evangelos Papadopoulos
Received his Diploma from the NTUA in 1981, and his M.S. and Ph.D. from MIT in 1983 and 1991 respectively, all in ME. He then joined McGill U., ME Dept. where he became an Assoc. Prof. (1997). Currently, he is an Assoc. Prof. with the ME Dept. of NTUA. His research interests are in robotics, including forestry and space, modelling and control of dynamic systems, and electrohydraulic servo systems. He is a senior member of IEEE and AIAA and a member of ASME and Sigma Xi.

Yves Gonthier
Received his BS in 1993 and his M.Eng. in 1996 from McGill University, both in ME. From 1996-1997 he worked as a research engineer at the McGill Centre for Intelligent Machines and from 1997-1999 at the Centre de Recherche Informatique de Montreal (CRIM). He is currently with the Canadian Space Agency. His research interests include simulation of contact dynamics and of complex electromechanical and space systems.